

Supplementary Information for

The Balance of Electric Field and Interfacial Catalysis in

Promoting Water Dissociation in Bipolar Membranes

Zhifei Yan,^{1†} Liang Zhu,^{2†} Yuguang C. Li,¹ Ryszard J. Wycisk,³ Peter N. Pintauro,³ Michael
A. Hickner,² Thomas E. Mallouk¹

1 Departments of Chemistry, Biochemistry and Molecular Biology, and Physics, The Pennsylvania State University, University Park, Pennsylvania 16802, United States

2 Department of Materials Science and Engineering, The Pennsylvania State University, University Park, Pennsylvania 16802, United States

3 Department of Chemical and Biomolecular Engineering, Vanderbilt University, Nashville, TN 37235, United States

[†]These authors contributed equally to this work

*Corresponding author email: tem5@psu.edu

Materials

The commercial bipolar membranes used in this study were purchased from Fumatech FBM (Germany) with a thickness of around 150 μm ; Nafion 117 dispersion (5%, in alcohol and water) was purchased from Sigma-Adrich; PPO (polyphenylene oxide), NMP (N-methyl-2-pyrrolidone), N,N-dimethylhexylamine, DMF (dimethylformate) and PDDA (polydiallyldimethylammonium chloride) were used as received from Sigma-Adrich; GO suspension (1 mg/mL, in water) was prepared following the method described by Kovtyukhova et al.¹ Platinum wire (0.5 mm in diameter, 99.95%) was purchased from Alfa Aesar. Ag/AgCl (with 3 M NaCl filling solution) reference electrodes were purchased from BASI (MF-2052). All electrolytes were prepared using distilled and ion exchanged water (18.2 M Ω -cm) obtained from a Milli-Q Academic (model A10) water purifier.

Membrane Fabrication.

AEL Preparation.^{2,3} Brominated PPO with a DF (degree of functionalization) of 60 (2.5 g, 14.88 mmol) was dissolved in 30 mL of NMP. Then, N,N-dimethylhexylamine (0.52 g, 4.02 mmol) was added slowly. The mixture was stirred at room temperature for 48 h. N,N,N',N'-tetramethyl-1,6-hexamediamine (0.51 g, 2.95 mmol) was added to the resulting mixture. Subsequently, the solution was cast onto a levelled glass plate, and dried at 82 °C under ambient pressure for 24 h followed by vacuum drying for 24 h at 80 °C to give a ~100 μm thick, transparent, tough film. The resulting membrane was X27Y33 (33% diamine crosslinked) in the bromide form, where 27 represents total mol % of Br groups being reacted with N, N-dimethylhexamine and 33 represents total mol % of Br groups being reacted with N,N,N',N'-tetramethyl-1,6-hexamediamine.

BPM Preparation. Customized bipolar membranes were prepared with solvent-exchanged Nafion solution, GO and a cross-linked AEL (anion exchange layer). Exchanging alcohol and water in the as-received Nafion solution with DMF (dimethylformate) followed the procedure described in the literature.⁴ Briefly, 20 mL of Nafion solution dissolved in a short chain alcohol mixture was heated under vacuum in a water bath set at 50 °C, until the volume of the remaining solution was about 10% of the starting solution. Then 20 mL of DMF was added to the solution. The mixture was placed under vacuum at 80 °C. This process was repeated five times to ensure complete solvent exchange. The final 20 mL of solution was 5 % Nafion in DMF, denoted as DMF-Nafion. A bipolar membrane was fabricated by mounting a 3 cm × 3 cm AEL onto a glass substrate with double-sided tape. The edges of the exposed side of the AEL were covered with Kapton tape to mask a 2 cm × 2 cm area. The AEL was then modified with GO solution by layer-by-layer (LBL) assembly. A certain amount of GO solution (about 5 mL) was cast to cover the exposed AEL surface and left to stand for 20 minutes. After washing thoroughly with nanopure water, 5 mL of PDDA solution ($M_w = 1.2 \times 10^5$, 20 wt% in water), acting as polycation, was deposited onto the GO modified AEL. More layers of GO solution were cast if more than one layer of GO was desired. For BPM without catalyst (0GO BPM), less than 5 μL of GO solution was added to lower the resistance and to provide a better comparison with the BPMs with catalyst. The small amount of GO allows us to safely ignore the GO catalytic effect. After GO deposition, 400 μL of DMF-Nafion solution was cast onto the GO-modified AEL and the assembly was heated to 120 -130 °C on a hot plate for one hour to achieve higher cation conductivity in the Nafion CEL. The bipolar membrane was then placed in a convection oven at 60 °C overnight before it was finally stored in 0.5 M KNO_3 solution before testing.

2.3 Membrane Characterization. The cross-section of the customized bipolar membranes was characterized using field emission scanning electron microscopy (FESEM, FET NanoSEM 630, accelerating voltage 10 kV).

2.4 Electrochemical Characterization of the Membranes. The direct current (DC) current density-voltage curve, J-E curve, was carried out in a four-compartment electrochemical cell, as shown in Figure S1. The BPM was subjected to a given current in the center of the cell, while two auxiliary membranes, one AEM and one CEM, were placed on each side of the test membrane to minimize the influence of the electrochemical reaction products at the working and counter electrodes. Two Pt wires, serving as working and counter electrodes, were used to apply current in the two outside chambers, while two Ag/AgCl reference electrodes were fixed in the two middle chambers using Haber-Luggin capillaries. The CEL of the studied BPM was in contact with 0.5 M HCl solution, and the AEL side was in contact with 0.5 M NaOH solution. Electrolyte solution was flowed through the cathode and anode chambers using a peristaltic pump.

Prior to the J-E curve measurements, the BPMs were conditioned in pure water overnight. Galvanostatic steps were applied for 5 minutes at each current density to allow the membrane to achieve steady state. The potential drop across the BPM was then recorded as the potential difference between the two reference electrodes. Reported results were averaged from three repeats.

Electrochemical impedance spectroscopy (EIS) measurements of the BPMs were conducted with the same setup. However, 0.5 M KNO₃ was used as the electrolyte in both the cathode and anode compartments. During the measurements, the flow of electrolyte was paused by stopping the peristaltic pump in order to achieve a better signal-to-noise ratio. Before incrementing to the next current density, the pump was used to refresh the electrolytes, which

ensured the same starting conditions for all measurements. Moreover, the system was subjected to the targeted DC current for 10 minutes to reach an equilibrium state prior to applying the AC input signal.

EIS experiments were conducted using an Autolab (PGSTAT128N), in galvanostatic mode with a frequency response analyzer (Metrohm, Netherland), in the frequency range of alternating current from 5 mHz to 100 kHz distributed uniformly on the logarithmic scale. The amplitude of the AC input signal was adjusted accordingly at a given DC current to ensure both a good signal-to-noise ratio and the absence of distortion in the signal as confirmed by symmetric Lissajous plots. EIS data were fitted by a complex nonlinear least-squares algorithm using the Zview 3.0 software package.

Four-Compartment Setup

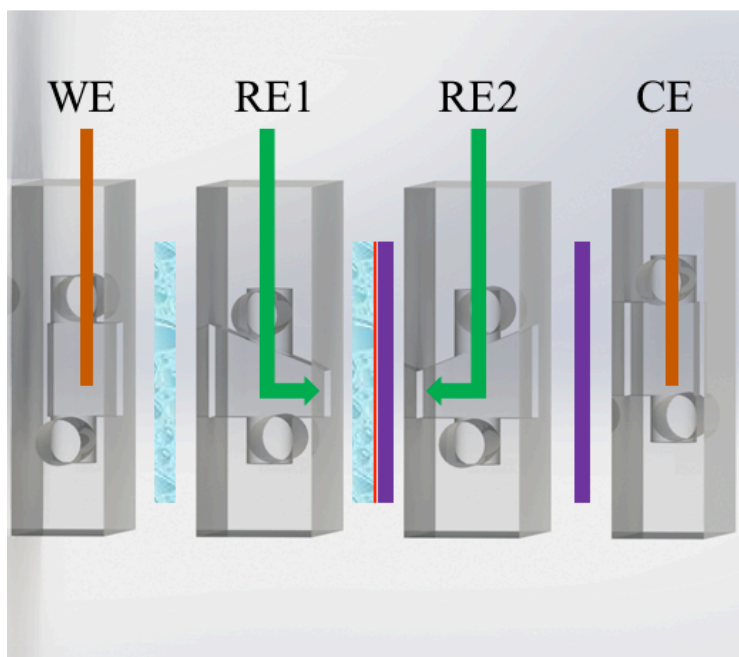


Figure S1. Setup for measuring BPM performance. WE: working electrode, Pt wire (0.5 mm diameter), CE: counter electrode, Pt wire (0.5 mm diameter); RE1 and RE2: reference electrode, Ag/AgCl with 3 M NaCl filling solution. The membranes were arranged, from left to right: CEM (blue), BPM (blue and purple) and AEM (purple), with the cathode located on the left side. The two monopolar membranes were incorporated to minimize the effects of water splitting products (H_2 and O_2) generated at the working and counter electrodes.

Equivalent Circuit

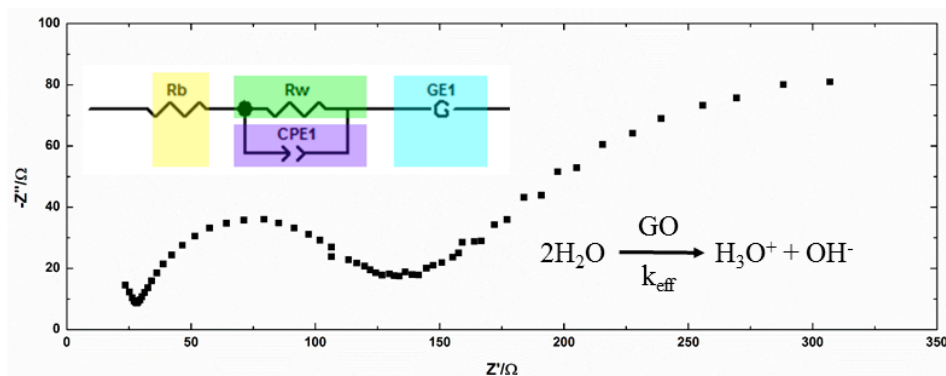


Figure S2. The equivalent circuit (EC) used to fit experimental EIS spectra.

The EC consists of a series connection of a resistor R_b which represents the resistance from the membrane and electrolyte bulk, Gerischer impedance $GE1$ and a block of a resistor R_w and a constant phase element (CPE) $CPE1$ connected in parallel.⁵

The Gerischer impedance $GE1$ couples the diffusion process to a chemical reaction that reacts as a sink or source to the studied species.^{5,6}

$$\frac{\partial \delta c_{H^+}}{\partial t} = D_{H^+} \frac{\partial^2 \delta c_{H^+}}{\partial x^2} + k_e \delta c_{H^+} \quad (S1)$$

where D_{H^+} and δc_{H^+} are the diffusion coefficient and change in H^+ concentration, and k_e is the effective water dissociation rate constant. Under semi-infinite boundary conditions, the solution to equation S1 follows:

$$Z = \frac{R}{\sqrt{2}} \times \left(\sqrt{\frac{1}{\sqrt{a}} + \frac{1}{a}} - j \sqrt{\frac{1}{\sqrt{a}} - \frac{1}{a}} \right) \quad (S2)$$

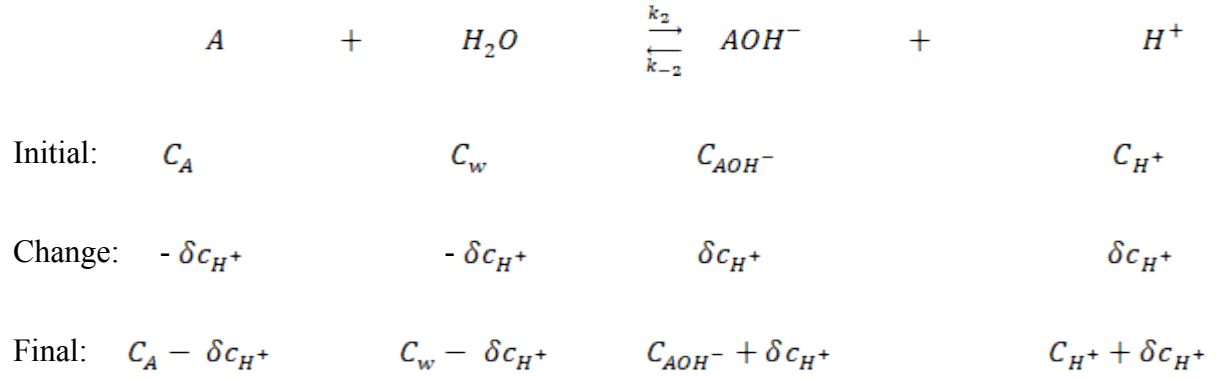
$$R = \frac{R_{gas} T}{F^2 \delta c_{H^+} \sqrt{D_{H^+} + k_e}} \quad (S3)$$

$$\alpha = \left(\frac{\omega}{k_g}\right)^2 + 1 \quad (\text{S4})$$

where ω is the applied frequency and R_{gas} , T , and F are the gas constant, temperature and Faraday constant, respectively. Considering that the protonation-deprotonation mechanism is catalyzed by a base, as was proposed by Simon:⁷



We assumed that the EIS AC input signal produces a transient change in H^+ concentration, δc_{H^+} . Then, by applying a chemical equilibrium analysis,



The reaction rate can then be expressed as:

$$R_{c_{H^+}} = k_2(C_A - \delta c_{H^+})(C_w - \delta c_{H^+}) - k_{-2}(C_{AOH^-} + \delta c_{H^+})(C_{H^+} + \delta c_{H^+}) = (k_2 C_w + k_{-2}(C_{AOH^-} + C_{H^+}))\delta c_{H^+} = k_e \delta c_{H^+} \quad (\text{S6})$$

In writing the last two equations, we eliminated the infinitely small terms and assumed that the water concentration is not affected appreciably.

Equation S6 supports the idea that the second term on the right side of equation S1 is the net product of water dissociation. Below the formal potential, -0.83V at room temperature, the water dissociation reaction will not produce net products. However, as pointed out by Hurwitz and Dibiani,⁵ the acid or base catalyst in the reaction layer is able to hold H^+ and

OH⁻ up to a frequency range as high as 1 MHz, so all the changes in c_{H^+} within the reaction layer are virtual changes. As a result, the dissociation reaction constant at the formal potential is also virtual in the sense that it does not produce any real concentration changes. As such, the rate constant k_d can be viewed as characterizing the forward reaction rate constant of water dissociation, k_s . The parameter that we extract from the Gerischer element **GE1** is thus the forward rate constant k_d .

The current across the reaction layer is composed of two sources: electrical double layer (EDL) charging current and water dissociation current. The former was represented by a constant phase element (CPE) due to the heterogeneity at the AEL/CEL interface. The latter was modelled by a resistor R_w that gives the resistance of the water dissociation reaction at various biases. The equivalent capacitance is estimated from the CPE using the relation:

$$C = R_w^{(1-n)/n} Q^{1/n} \quad (S7)$$

$$Z_{CPE} = \frac{1}{Q(j\omega)^n} \quad (S8)$$

where Q and n are the pseudo-capacitance and CPE order, respectively, as extracted from the CPE element.

Electrochemical Impedance Spectroscopy (EIS) Measurements

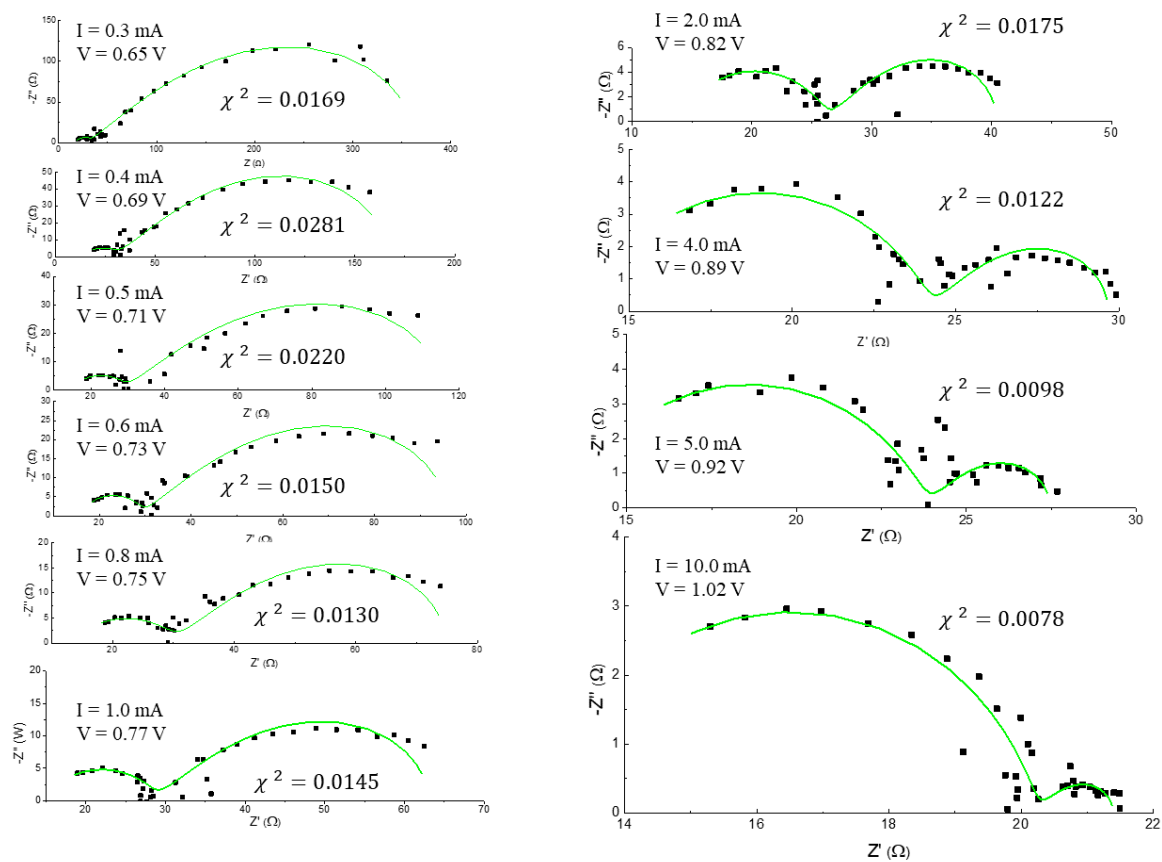


Figure S3. Experimental (black squares) and modelled (green lines) Nyquist plots of BPM with 4 layers of GO, 4GO BPM at different reverse bias potentials. The equivalent circuit is described in Figure S2.

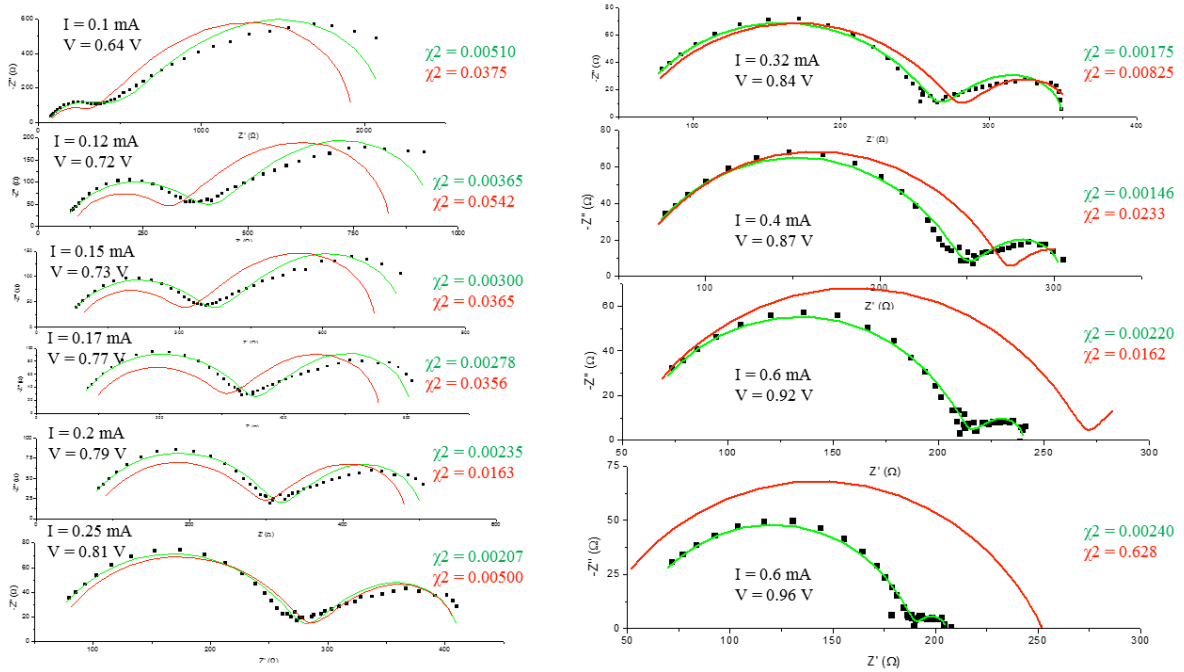


Figure S4. Experimental (black squares) and modelled (green lines) Nyquist plots of BPM with no GO, 0GO BPM at different **reverse bias** potentials. The red lines are modeled spectra with a fixed depletion layer thickness. Specifically, the depletion layer thickness at various potentials are averaged for the 0GO BPM. We then repeated the EIS modeling at the fixed (average) depletion thickness while other parameters were allowed to float freely. This fitting scheme (red lines) shows that the chi squared values are in the range of 0.03-0.6, which is much larger than that of the fitting at individually optimized depletion layer thicknesses (green lines).

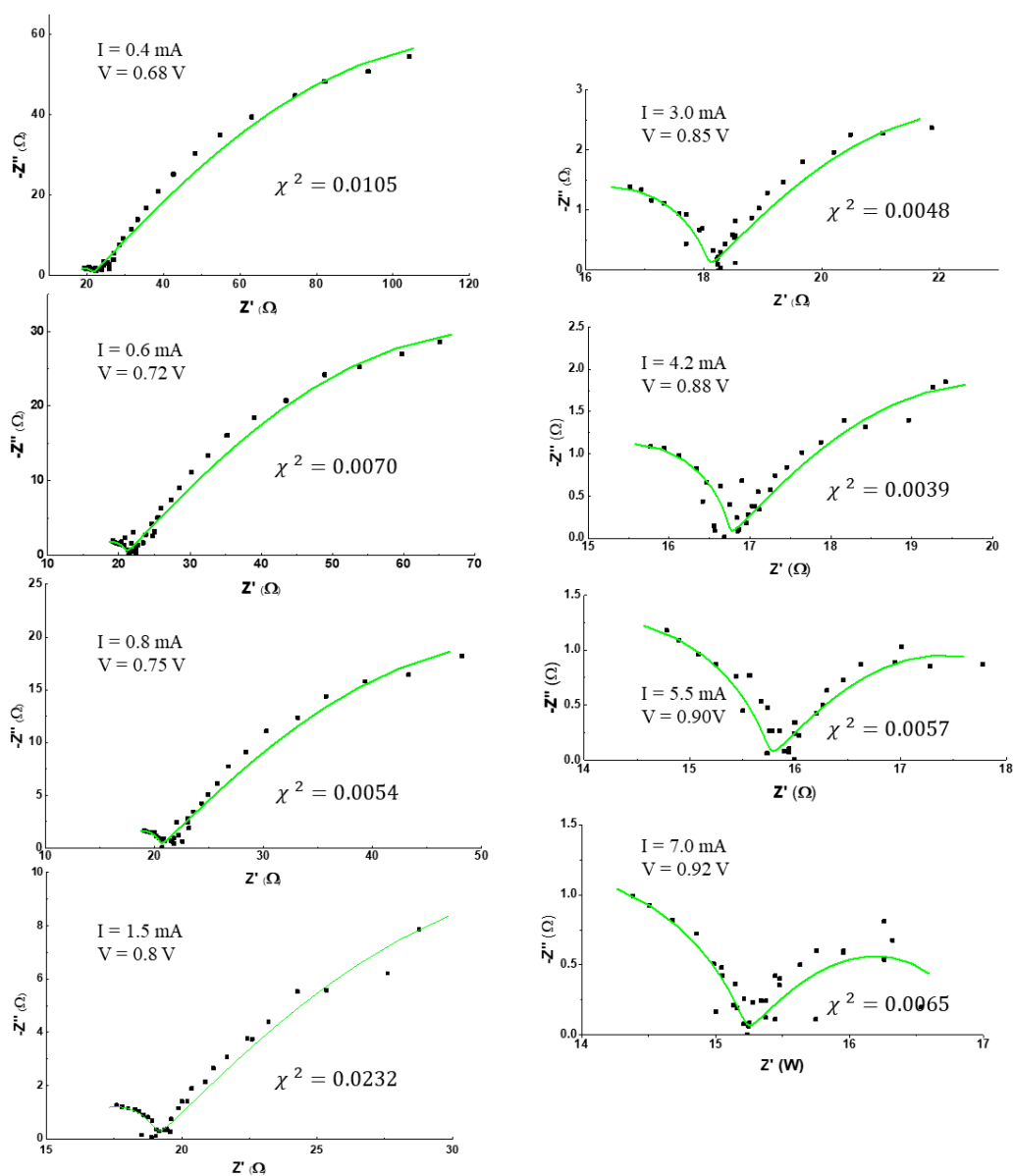


Figure S5. Experimental (black squares) and modelled (green lines) Nyquist plots 3D BPM at different reverse bias potentials.

Determination of the Depletion Layer Thickness from EIS

To calculate the depletion layer thickness, the experimental EIS spectra were first fitted to the equivalent circuit in Fig. S2, as was done in Fig. S3, S4 and S5 for 4GO/0GO and 3D BPMs. The extracted parameters were those related to R_b representing the bulk resistance, the Gerischer element GE1 representing the reaction-coupled diffusion process (equations S1-S4), R_w the water dissociation resistance, and a CPE representing the electric double layer.

In the fitting software package, the Gerischer element has two parameters: GET and GEP, corresponding to R (Ω , equation S3) and k_e ($=k_d, s^{-1}$). The CPE element has two parameters: CPET and CPEP, corresponding to Q and n in Equation S8. The parameter n is a unitless number, and as the overall units of Z are Ω . The Q parameter has units of $\Omega^{-1} \cdot s^n$. The capacitance is thus calculated according to equation S7, from which the depletion layer thickness d can be obtained by using equation 2 in the main text.

As a critical analysis, one may recall that the equation used to calculate the depletion layer thickness is derived for two parallel plates of area A separated by a distance d . Strictly speaking, the depletion region considered here, as depicted in Fig. 4, is not a conventional plate capacitor because the depletion region has a finite thickness. However, the equivalent circuit we used to model the process is a constant phase element CPE, which is meant to simulate processes in which a large heterogeneity exists. As shown in Fig. S9 below, there is indeed a large decay of the net charge density from the middle to the edge of the depletion region, indicating a non-uniform distribution of charge in the “capacitor”. More importantly, as a general rule, a CPE resembles an ideal capacitor when the n parameter (CPEP) approaches 1. This is indeed the case by comparing the n parameters for the 3D BPM, ~ 0.9 (Table S4), to that of the 0GO BPM, $\sim 0.6-0.7$ (Table S3). The former has a much thinner

depletion region (Fig. 5), and one may imagine that the thin depletion region in the 3D BPM makes it structurally resemble the planar capacitor, and thus have close to unit n parameters.

Table S1. Parameters extracted from EIS and calculated values of capacitance and depletion layer thickness for 4GO BPM

Reverse current (mA/cm ²)	Cross membrane potential (V)	Rb (Ω)	GET (X10 ⁴ , Ω ⁻¹)	GEP (kd, s ⁻¹)	Rw (Ω)	CPET (x10 ⁵) ^a	CPEP	Capacitance (x10 ⁶ , F) ^b	Depletion layer thickness (nm) ^c
0.3	0.64 (0.012) ^d	15.67 (1.44)	37.71 (7.29)	1.03 (0.08)	16.68(6.36)	5.41(5.38)	0.75(0.16)	2.81(0.50)	25.70(4.16)
0.4	0.69	13.72 (0.15)	67.36 (3.17)	1.30 (0.02)	17.22(0.71)	10.46(3.73)	0.61(0.04)	1.60(0.04)	44.36(1.20)
0.5	0.71	14.78 (2.07)	101.35 (5.39)	1.32 (0.14)	16.28(1.69)	5.18(4.02)	0.71(0.09)	2.13(0.65)	35.86(12.62)
0.6	0.73	14.26 (1.39)	139.66 (18.11)	1.39 (0.07)	16.70(2.03)	6.34(4.80)	0.67(0.08)	1.79(0.26)	40.20(6.28)
0.8	0.75	13.15 (1.04)	204.02 (18.25)	1.28 (0.23)	18.10(2.61)	9.61(5.35)	0.62(0.08)	1.63(0.19)	43.85(4.74)
1.0	0.77	13.22 (1.41)	254.67 (12.72)	1.36 (0.11)	15.70(2.04)	5.76(2.83)	0.67(0.08)	1.68(0.51)	45.34(16.23)
2.0	0.82	14.65 (0.59)	537.59 (27.47)	1.71 (0.13)	11.36(0.46)	2.14(0.79)	0.79(0.05)	2.25(0.37)	32.02(4.93)
3.0	0.86	15.19 (0.21)	774.94 (24.76)	2.00 (0.11)	9.23(0.15)	0.73(0.07)	0.91(0.02)	2.87(0.43)	24.99(3.75)
4.0	0.89	13.50 (0.54)	1473.43 (148.13)	1.92 (0.24)	10.80(0.64)	2.55(0.53)	0.77(0.03)	2.07(0.27)	34.69(4.92)
5.0	0.92	13.58 (0.70)	1795.17 (123.71)	2.20 (0.48)	9.98(0.92)	2.45(1.28)	0.79(0.08)	2.32(0.50)	31.33(5.99)
10	1.02	12.55 (0.37)	5896.47 (198.90)	2.94 (1.14)	7.90(0.58)	1.90(0.70)	0.81(0.04)	2.17(0.31)	33.19(5.06)
20	1.17	9.81 (1.13)	e		7.08(1.25)	1.98(0.74)	0.76(0.07)	1.20(0.59)	74.06(47.10)
30	1.30 (0.006)	8.29 (0.29)			6.59(0.26)	1.45(0.01)	0.76(0.01)	0.74(0.08)	96.21(10.19)

a. The unit of CPET is Ω⁻¹.s^{CPEP};

b. Capacitance is calculated according to equation S7;

c. Depletion layer thickness is calculated based on equation 2 in the main text.

d. Values in the bracket indicate the standard deviation in a set of three repeated measurements. Standard deviations of < 1 % of the average values are not labeled in the table.

e. Extracting accurate values of kd at reverse potential > 1.1 V were not successful because the lower frequency semicircles in the EIS spectra become small and noisy at those biases (Fig. S3 and S4)

Table S2. Parameters extracted from EIS and calculated values of capacitance and depletion layer thickness for 1GO BPM

Reverse current (mA/cm ²)	Cross membrane potential (V)	Rb (Ω)	GET (X10 ⁴ , Ω ⁻¹)	GEP (kd, s ⁻¹)	Rw (Ω)	CPET (x10 ⁵)	CPEP	Capacitance (x10 ⁶ , F)	Depletion layer thickness (nm)
0.25	0.64 (0.05)	22.57 (1.06)	26.19 (13.88)	0.75 (0.06)	36.03(9.35)	1.28(0.58)	0.79(0.07)	1.54(0.21)	46.55(5.91)
0.30	0.68 (0.03)	22.25 (1.22)	40.69 (14.06)	0.81 (0.01)	35.92(7.06)	1.37(0.47)	0.77(0.04)	1.28(0.07)	55.36(3.24)
0.40	0.71 (0.01)	20.78 (1.38)	70.49 (12.02)	0.99 (0.14)	35.25(3.17)	2.11(0.97)	0.71(0.07)	1.04(0.22)	70.10(15.75)
0.50	0.74 (0.01)	19.33 (2.05)	106.79 (10.51)	0.88 (0.03)	36.81(2.39)	3.31(1.66)	0.67(0.08)	0.97(0.28)	76.85(21.54)
0.70	0.76 (0.01)	21.62 (1.70)	168.03 (19.66)	0.96 (0.05)	30.28(3.84)	1.36(0.60)	0.76(0.05)	1.04(0.23)	70.40(15.40)
1.0	0.80	20.38 (0.39)	264.20 (13.80)	1.16 (0.12)	27.99(0.95)	1.59(0.20)	0.74(0.02)	0.99(0.18)	73.29(14.58)
2.0	0.86	20.20 (0.51)	642.24 (14.89)	1.54 (0.02)	21.99(0.96)	1.03(0.19)	0.79(0.02)	1.05(0.12)	67.79(7.44)
3.0	0.91	19.13 (0.44)	1126.23 (54.44)	2.11 (0.13)	19.70(0.17)	0.98(0.03)	0.79(0.01)	1.01(0.11)	70.80(8.26)
4.0	0.94 (0.01)	19.36 (0.24)	1452.97 (126.96)	3.56 (0.69)	16.24(0.33)	0.76(0.07)	0.83(0.01)	1.18(0.01)	59.91(0.60)
10	1.11	15.30 (0.21)			11.50(0.31)	0.65(0.09)	0.83(0.02)	0.96(0.04)	73.63(3.33)
20	1.29	11.54 (0.07)			9.38(0.08)	0.43(0.02)	0.83	0.56(0.02)	126.77(4.57)
30	1.44	8.69 (0.06)			9.19(0.09)	0.21(0.01)	0.84(0.02)	0.27(0.08)	283.52(103.3)

Table S3. Parameters extracted from EIS and calculated values of capacitance and depletion layer thickness for 0GO BPM

Reverse current (mA/cm ²)	Cross membrane potential (V)	Rb (Ω)	GET (X10 ⁴ , Ω ⁻¹)	GEP (kd, s ⁻¹)	Rw (Ω)	CPET (x10 ⁵)	CPEP	Capacitance (x10 ⁶ , F)	Depletion layer thickness (nm)
0.10	0.63 (0.02)	40.54 (1.98)	6.95 (1.8)	0.58 (0.10)	437.23(20.10)	2.77(0.44)	0.55(0.01)	0.80(0.12)	90.41(13.24)
0.12	0.72 (0.01)	52.16 (0.49)	22.80 (16.9)	0.62 (0.04)	345.10(7.34)	1.00(0.04)	0.65	0.47(0.01)	149.38(2.97)
0.15	0.73 (0.01)	52.44 (0.93)	29.07 (19.2)	0.71 (0.01)	311.53(3.03)	0.94(0.08)	0.66(0.01)	0.44	160.06(1.50)
0.17	0.77	55.12 (0.53)	47.12 (16.5)	0.67 (0.07)	286.07(8.01)	2.74(3.54)	0.69(0.01)	4.07(6.33)	117.37(96.25)
0.20	0.79	54.90 (0.44)	59.81 (0.77)	0.86 (0.02)	255.47(2.72)	0.61(0.01)	0.70	0.39	180.49(0.74)
0.25	0.81	53.92 (0.33)	83.18 (4.02)	0.90 (0.09)	224.20(6.15)	0.57(0.02)	0.71	0.38	187.42(2.20)
0.32	0.84	54.26 (0.32)	120.90 (2.40)	0.98 (0.07)	210.77(1.78)	0.49(0.01)	0.73	0.37	192.80(0.27)
0.40	0.87	53.20 (0.47)	169.59 (5.21)	1.10 (0.03)	195.07(1.88)	0.46(0.02)	0.73	0.36	198.63(0.58)
0.60	0.92	52.09 (1.67)	309.93 (10.82)	1.48 (0.11)	161.40(0.79)	0.39(0.06)	0.75	0.34(0.01)	206.63(8.70)
0.80	0.96	48.52 (0.40)	525.54 (21.38)	1.86 (0.21)	141.80(0.44)	0.41(0.02)	0.74(0.01)	0.31	227.35(2.32)
1.00	0.99	47.33 (0.06)	759.37 (88.56)	2.39 (0.31)	125.15(0.49)	0.37	0.75	0.30	233.94(2.55)
2.00	1.12	40.03 (0.94)			86.58(1.07)	0.33(0.03)	0.75(0.01)	0.24(0.01)	300.76(14.44)
4.00	1.29	31.54 (0.47)			59.97(0.24)	0.24(0.01)	0.77	0.17	404.97(2.10)
8.00	1.53	20.98			46.02	0.16	0.78	0.80	690.41

Table S4. Parameters extracted from EIS and calculated values of capacitance and depletion layer thickness for 3D BPM

Reverse current (mA/cm ²)	Cross membrane potential (V)	Rb (Ω)	GET (X10 ⁴ , Ω ⁻¹)	GEP (kd, s ⁻¹)	Rw (Ω)	CPET (x10 ⁵)	CPEP	Capacitance (x10 ⁶ , F)	Depletion layer thickness (nm)
0.4	0.68	17.89 (0.31)	216.59 (2.16)	0.07 (0.01)	3.25(0.36)	2.01(0.88)	0.98(0.05)	15.41(2.71)	4.69(0.79)
0.6	0.72	17.14 (0.55)	400.16 (4.67)	0.09	3.44(0.36)	1.05(0.19)	0.99(0.02)	9.78(3.56)	8.09(3.50)
0.8	0.75 (0.01)	16.82 (0.59)	581.73 (3.09)	0.09	3.49(0.65)	4.91(6.86)	0.98(0.07)	25.10(23.72)	4.91(3.62)
1.5	0.80	15.27 (1.69)	1441.57 (17.94)	0.09 (0.01)	3.65(1.92)	3.34(2.28)	0.87(0.18)	9.30(7.93)	26.50(36.17)
3.0	0.85	14.19 (1.19)	3643.60 (55.13)	0.13 (0.01)	3.31(0.79)	2.72(1.53)	0.86(0.10)	5.65(2.95)	16.69(12.06)
4.2	0.88	14.03 (0.26)	5536.40 (372.45)	0.14 (0.04)	2.79(0.44)	2.78(1.95)	0.88(0.08)	6.85(1.90)	10.89(3.01)
5.5	0.90	12.97 (0.71)	7269.87 (357.94)	0.26 (0.02)	2.78(0.58)	1.72(0.28)	0.90(0.06)	5.99(3.04)	15.28(10.34)
7.0	0.92	12.29 (0.66)	9838.43 (558.57)	0.35 (0.08)	2.91(0.62)	2.68(0.82)	0.85(0.85)	5.19(313)	16.70(7.63)

Numerical Model of the BPM

Model Formulation

The potential distribution and ionic transport can be described by coupling Poisson's equation and the Nernst-Planck equation.

$$\nabla(-D_i \nabla C_i - z_i u_i F C_i \nabla V) = R_i \quad (\text{S9})$$

$$\nabla(\varepsilon \varepsilon_0 E) = \rho_v \quad (\text{S10})$$

Where, E is the electric field, ε and ε_0 are the relative dielectric constant and the vacuum permittivity with a value of 8.854×10^{-12} F/m, respectively. The value of ε is taken as 80 for water. ρ_v is the net space charge density, which arises because of the concentration difference between cations and anions. D_i, u_i, C_i, z_i are the diffusion coefficient, mobility, concentration and charge of species i , respectively. V is the potential, the gradient of which is electric field. In equation S9, R_i , is the generation term describing contributions to concentration from the chemical reaction. In the BPM system, H^+ and OH^- are generated by the water dissociation reaction under reverse bias conditions, while the amount of supporting electrolyte is assumed to be conserved. The generation term for H^+ and OH^- is written as:

$$R_i = k_d C_{H_2O} - k_b C_{H^+} C_{OH^-} \quad (\text{S11})$$

where k_d is the dissociation rate constant and k_b the backward reaction rate constant, or the recombination rate constant. In writing the first term on the right side, we included a C_{H_2O} constant in k_d . Incorporating the catalyst is tantamount to increasing k_d by two orders of magnitudes in our model, i.e., 2×10^{-3} 1/s. These equations were programmed and solved with COMSOL v 5.1, using a finite element methodology. Time dependent studies of **at least 30 seconds** were allowed to reach steady states.

Electric Field and Catalytic Effect

As is discussed in the main body of the paper, electric field-enhanced water dissociation is taken into account by setting the forward reaction rate constant as a function of the electric field across the BPM junction, based on Onsager's weak electrolyte theorem:⁸

$$k_d = k_d(0) \times \frac{J_1\left(4\left(\frac{b}{2}\right)^{0.5}\right)}{2\left(\frac{b}{2}\right)^{0.5}} \quad (\text{S12})$$

$$b = 0.009636E/\varepsilon_r T^2 \quad (\text{S13})$$

where $k_d(0)$ is the dissociation rate constant without electric field, E is the electric field, T is the temperature, and J_1 is the Bessel function of the first type.

The mechanism of how the catalyst affects water dissociation has been discussed by Tuckerman et al.^{9,10} One of the most popular views accepts the protonation-deprotonation reaction, equation S5. A detailed version of a comprehensive model would explicitly consider the concentration of active catalytic sites and the catalytic reaction network.¹¹ Yet, the model proposed in the present study is able to capture the basic catalytic effect by increasing the effective forward reaction rate constant, as demonstrated in equation S6. The detailed mechanism of catalyzed water dissociation is then implied in the effective rate constant k_e . In principle, our model can be modified to describe a different water dissociation mechanism as long as the generation term R_i is able to be correlated with the proposed mechanism, such as through a detailed chemical equilibrium analysis.

Boundary Conditions and Initial Conditions

The model is a 1-D model composed of a 20 μm AEL and 20 μm CEL with 200 μm of electrolyte solution on both sides. The two layers of electrolyte are an important component of the model as experimentally there will always be some amount of solution between the tips of the reference electrodes (Figure S1), no matter how close they are placed to the membrane surface. The concentration of the supporting electrolyte KNO_3 is fixed to be 0.1 mol/m³ at the two boundaries, while the concentration of H^+/OH^- is fixed as 10⁻⁴ mol/m³, which is the concentration of these species in pure water. The low concentration chosen to ease the simulation cost may limit the H^+/OH^- flux at large reverse bias, as is discussed in the main text. The right boundary of the diffusion layer is set as ground and the targeted potential is imposed on the left boundary where the current density is collected based on the total flux of all the charged species. The initial values of relevant parameters in the simulation are listed in Table S1. The diffusion coefficients of H^+ and OH^- and dielectric constant are set to the smaller values than those in normal aqueous system.¹²⁻¹³ However, they simplify the interpretation of the results and can better describe the BPM system.¹³

Table S5 Initial conditions of the numerical simulation.

Parameter	Value	Description
$D_{\text{H}^+} / D_{\text{OH}^-}$	2e-10 m ² /s	Diffusion coefficients of H^+ and OH^-
$D_{\text{K}^+} / D_{\text{NO}_3^-}$	1e-10 m ² /s	Diffusion coefficients of K^+ and NO_3^-
$c_{\text{H}_2\text{O}}$	56 M	Concentration of water
$c_{\text{K}^+} / c_{\text{NO}_3^-}$	0.5 mM (In membrane) 0.1 mM (In electrolyte)	Concentration of supporting electrolyte
$c_{\text{H}^+} / c_{\text{OH}^-}$	1e-4 mM	Concentration of H^+ and OH^-
$k_d(0)$	2e-5 1/s	Forward reaction constant without electric field
ϵ_r	10	Relative dielectric constant

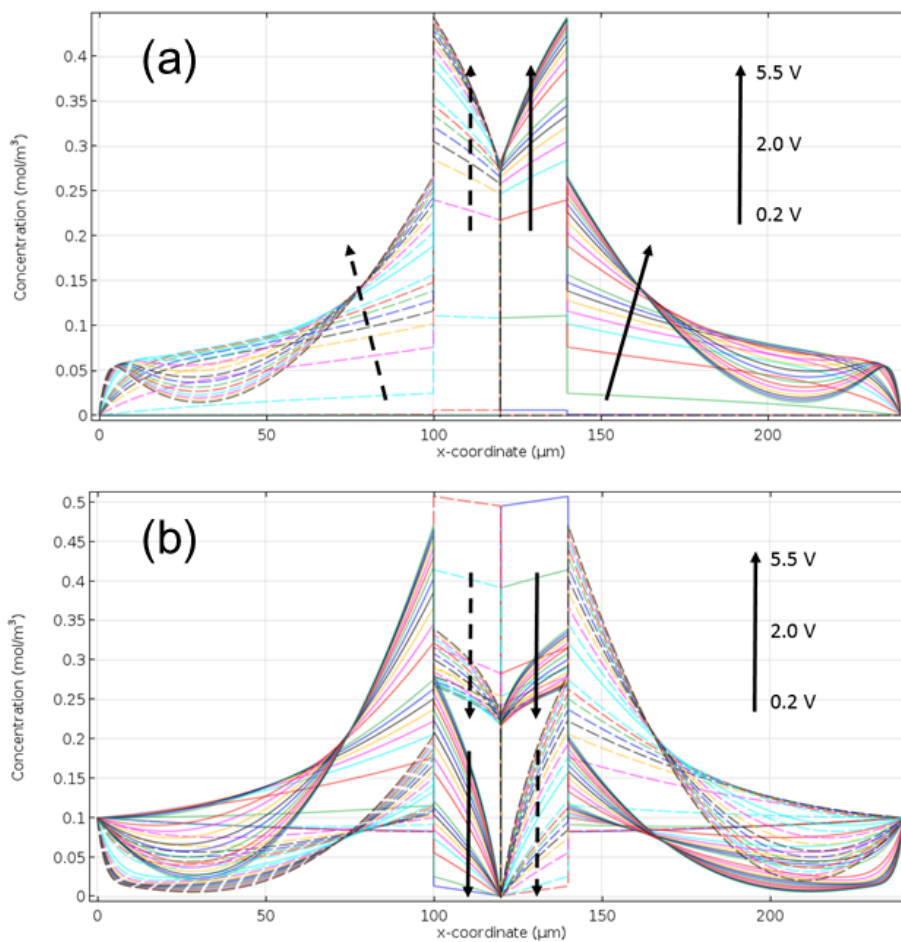


Figure S6. Concentration profiles of the ionic species obtained from simulation at all reverse biases, for the BPM with catalyst. (a) H⁺ (solid lines) and OH⁻ (dashed lines); (b) K⁺ (solid lines) and NO₃⁻ (dashed lines). The arrows indicate the profile evolution as the potential changes.

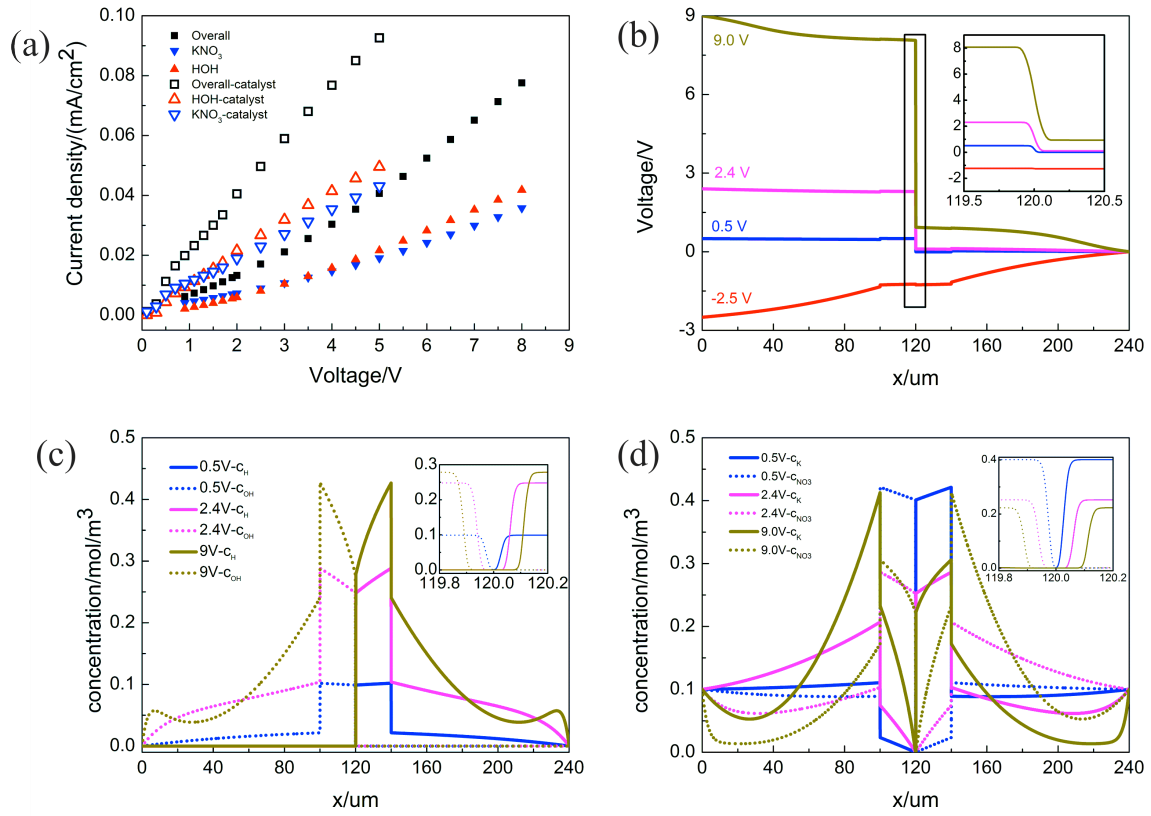


Figure S7. Simulated results of BPMs without catalyst. (a) J-E curves with (hollow) and without (solid) catalyst; (b) potential distribution of a BPM without catalyst; (c) Water dissociation products H⁺ and OH⁻ concentration distribution in the BPM; (d) Electrolyte KNO₃ ion distribution. Insets in (b) (c) and (d) are enlarged versions of the AEL/CEL junction region.

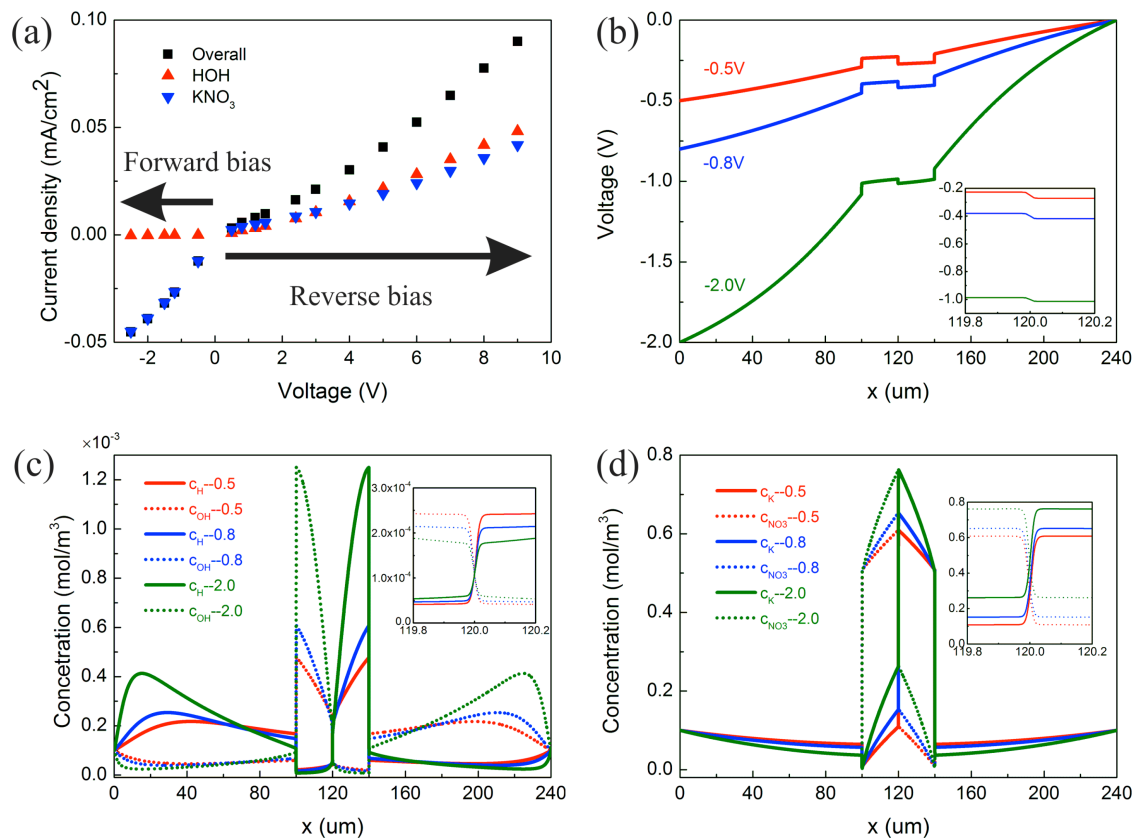


Figure S8. Simulated result of a BPM without catalyst under forward bias conditions. (a) J-E curve under forward and reverse bias conditions; (b) potential distribution under forward bias; (c) Water dissociation products H⁺ and OH⁻ concentration distributions in the BPM; (d) Electrolyte KNO₃ ion distribution. Note the absence of a depletion region under **forward bias** conditions. Insets in (b) (c) and (d) are enlarged version of the AEL/CEL junction region.

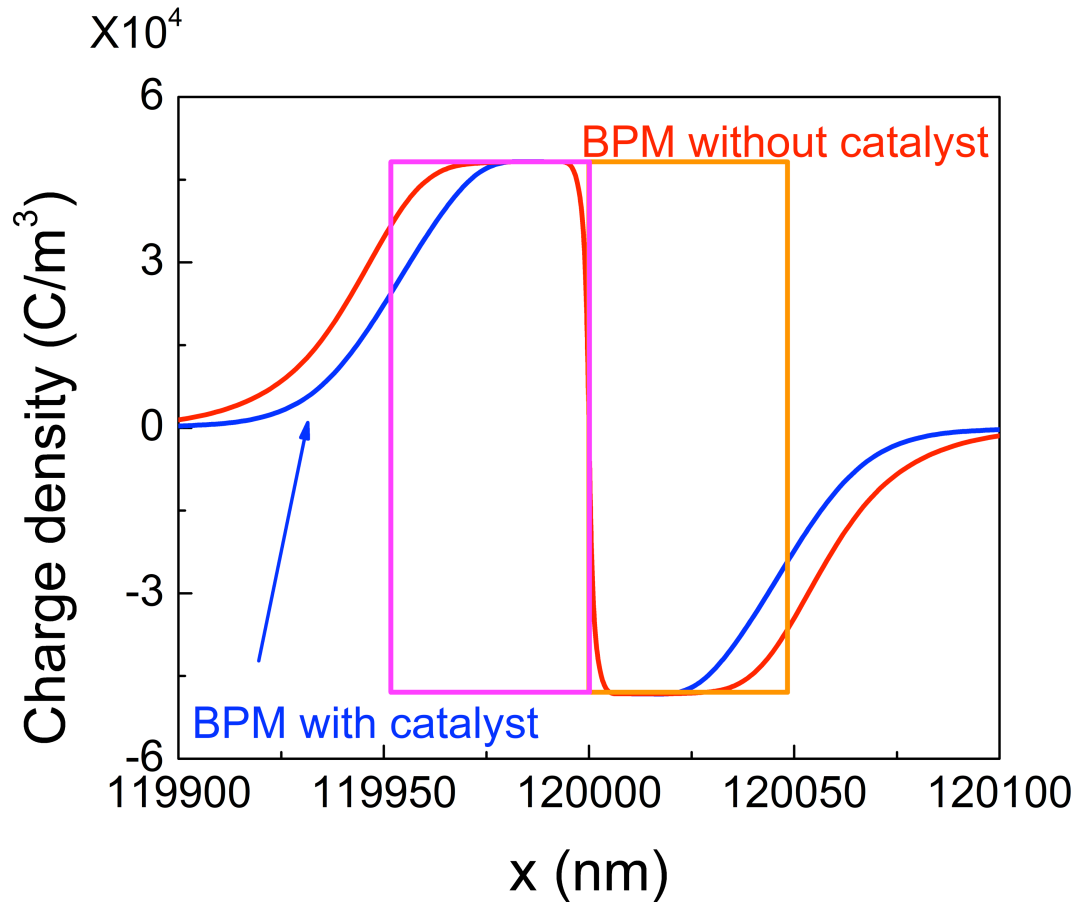
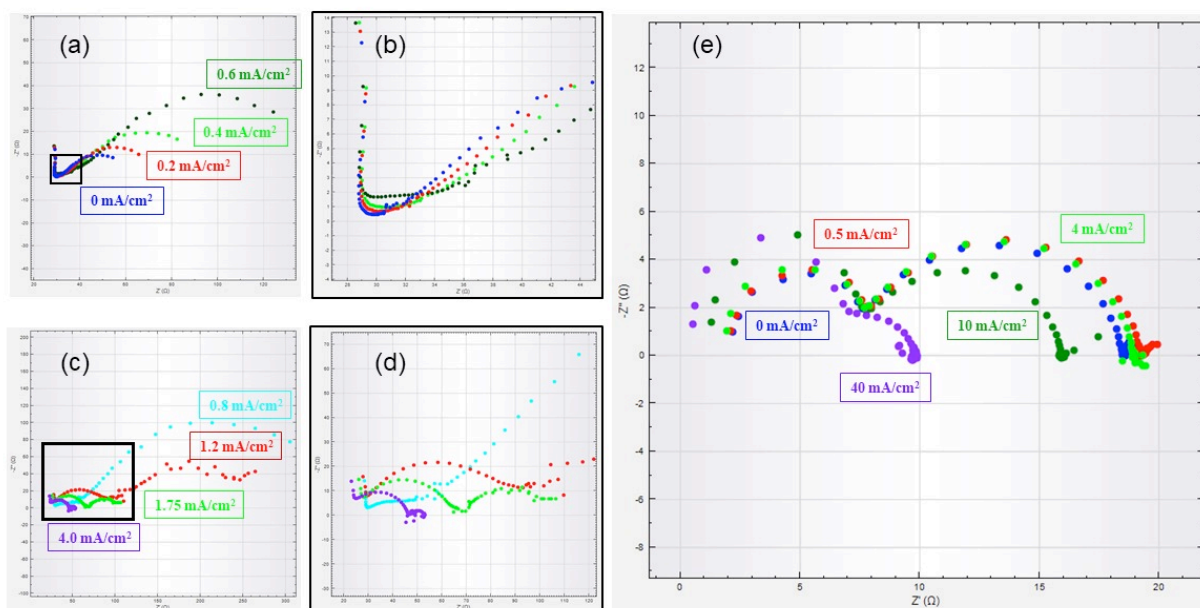


Figure S9. Determination of the depletion region thickness from simulation. The distance from the point where charge density drops to half of the maximum in the AEL to its counterpart point in CEL is taken as the depletion region thickness. The magenta and orange boxes represent the depletion region on the AEL and CEL sides, respectively. The depletion thickness in this case is the distance between the left side of the magenta box and the right side of the orange box. The two curves are for BPMs with and without catalyst at a reverse bias of 2 V, and the boxes representing the depletion layer are for BPM with catalyst.



Spectra taken in 0.5 M KNO_3 at both cathode and anode Chamber; galvanostatic mode, 50-100 μA , 10^5 -0.005 Hz

Spectra taken with 0.5 M HCl and 0.5 M KOH at the cathode and anode, respectively; galvanostatic mode, 50-100 μA , 10^5 -0.005 Hz

Figure S10. Comparison of the EIS spectra of the 1GO BPM taken in pH neutral (a-d) and asymmetric conditions (e). (a-d): with the pH neutral electrolyte 0.5 M KNO_3 , the gradual appearance of the intermediate semicircle as the reverse bias current increases is observed. (b) and (d) show an enlarged version of the intermediate semicircle in the square of Fig. (a)(c). From zero bias to 0.8 mA/cm^2 and above, the intermediate semicircle becomes more obvious, which confirms the gradual formation of the depletion region and the intensification of the water autodissociation reaction under the electric field. (e) Spectra taken under asymmetric conditions exhibit the intermediate semicircle even at open circuit, because of the intrinsic electric field across the AEL/CEL interface. The intrinsic electric field arises because of the acid-base neutralization reaction at the AEL/CEL interface, which leaves the fixed membrane charge near the interface unbalanced, i.e. the formation of a depletion region. As such, even though the asymmetric condition is more relevant to standard operating conditions for BPMs, it doesn't provide information on the depletion layer thickness and water dissociation kinetics below the open circuit voltage (ideally 0.834 V, assuming 1M fixed charge density in the

AEL and CEL). Thus, the asymmetric pH spectra do not inform us about the trend in the water dissociation reaction during the early stages of formation of the depletion region.

REFERENCES

- 1 N. I. Kovtyukhova, P. J. Ollivier, B. R. Martin, T. E. Mallouk, S. A. Chizhik, E. V. Buzaneva and A. D. Gorchinskiy, *Chem. Mater.*, 1999, **11**, 771–778.
- 2 J. Pan, J. Han, L. Zhu and M. A. Hickner, *Chem. Mater.*, 2017, **29**, 5321–5330.
- 3 L. Zhu, T. J. Zimudzi, Y. Wang, X. Yu, J. Pan, J. Han, D. I. Kushner, L. Zhuang and M. A. Hickner, *Macromolecules*, 2017, **50**, 2329–2337.
- 4 H.-L. Lin, T. L. Yu, C.-H. Huang and T.-L. Lin, *J. Polym. Sci. Part B Polym. Phys.*, 2005, **43**, 3044–3057.
- 5 H. D. Hurwitz and R. Dibiani, *J. Membr. Sci.*, 2004, **228**, 17–43.
- 6 E. Kniaginicheva, N. Pismenskaya, S. Melnikov, E. Belashova, P. Sistas, M. Cretin and V. Nikonenko, *J. Membr. Sci.*, 2015, **496**, 78–83.
- 7 R. Simons, *Nature*, 1979, **280**, 824–826.
- 8 L. Onsager, *J. Chem. Phys.*, 1934, **2**, 599–615.
- 9 M. E. Tuckerman, D. Marx and M. Parrinello, *Nature*, 2002, **417**, 925–929.
- 10 D. Marx, M. E. Tuckerman, J. Hutter and M. Parrinello, *Nature*, 1999, **397**, 601–604.
- 11 D. T. Conroy, R. V. Craster, O. K. Matar, L.-J. Cheng and H.-C. Chang, *Phys. Rev. E*, 2012, **86**, 056104.
- 12 K. N. Grew, J. P. McClure, D. Chu, P. A. Kohl and J. M. Ahlfield, *J. Electrochem. Soc.*, 2016, **163**, F1572–F1587.
- 13 H. Strathmann, J. J. Krol, J. J. Rapp and G. Eigenberge, *J. Membr. Sci.* 1997, **125**, 123–142.